



# Lower limit analysis of active earth pressure of cohesionless soil with finite width

Hao Wu\*, Zhipei Zhang

Yellow River Engineering Consulting Co., Ltd., Zhengzhou, Henan 450003, China

\*250320158@qq.com

**Abstract.** The earth pressure with finite width is often encountered in engineering. Theoretical research and engineering practice show that the classical Rankine and Coulomb equations are not suitable for active earth pressure with finite width. In this paper, based on the lower bound theorem in plastic mechanics, the lower bound model for the active earth pressure of cohesionless soil with finite width is created, and the corresponding numerical solution method is provided. The active earth pressures and the distributions under different soil heights are calculated and analyzed. The results indicate that the active earth pressure of cohesionless soil with finite width is smaller than the corresponding Coulomb active earth pressure. As the burial depth of the soil increases, the active earth pressure and vertical friction between the soil and the wall continue to increase. Finally, the weight of the soil and the vertical friction between the soil and the wall reach an equilibrium state, and the soil pressure tends to a limit value. The calculation results and methods in this article can provide useful reference and guidance for the calculation of earth pressure.

**Keywords:** Lower bound theorem; Cohesionless soil; Limited width; Active earth pressure; Lower bound model; Numerical solution

## 1 Introduction

The calculation of earth pressure is a classic problem in soil mechanics and a current hot topic in theoretical and engineering research in the field of soil mechanics<sup>[1]</sup>. The classical Rankine and Coulomb earth pressure calculation theories and methods are widely adopted due to their clear concepts and computational simplicity, assuming semi-infinite soil mass behind the retaining wall during calculations<sup>[2]</sup>. However, in engineering practice, problems often arise involving finite-width earth pressure, such as in backfilled road embankments in mountainous areas and deep excavation support structures near adjacent buildings<sup>[3-6]</sup>. Both theoretical studies<sup>[7-9]</sup> and engineering practice<sup>[10]</sup> have shown that the classical Rankine and Coulomb earth pressure theories are not well-suited for the calculation of active earth pressure within finite widths.

© The Author(s) 2023

H. Bilgin et al. (eds.), *Proceedings of the 2023 5th International Conference on Civil Engineering, Environment Resources and Energy Materials (CCESEM 2023)*, Advances in Engineering Research 227,

[https://doi.org/10.2991/978-94-6463-316-0\\_27](https://doi.org/10.2991/978-94-6463-316-0_27)

The main reason for this maladaptation is that Rankine or Coulomb earth pressure assumes that the soil is sufficiently wide or infinitely wide, and the actual earth pressure is directly related to the width of the soil within a certain range. Only when the width of the soil exceeds the plastic range of active earth pressure, the active earth pressure is independent of the soil width.

In this paper, based on the lower bound theorem in plastic mechanics, we establish a lower bound model, provide a numerical solution for the lower bound model, and numerically solve the problem of active earth pressure produced by cohesionless fill soil within a finite width. This study aims to provide references for engineering practice and relevant theoretical research.

## 2 Lower Bound Model

### 2.1 Lower Bound Theorem

For ideal rigid-plastic materials, the lower bound theorem can be stated as follows: any static equilibrium stress field constitutes a lower bound solution for the ultimate load. A static equilibrium stress field refers to a stress field that simultaneously satisfies the following conditions:

- (a) Equilibrium equations;
- (b) Stress boundary conditions;
- (c) Yield criterion constraints.

### 2.2 Lower Bound Model

Assuming that  $V$  represents the study domain and  $S$  represents its surface, the lower bound model can be expressed as follows:

$$\left. \begin{array}{l} \max \quad Q(\sigma) \\ \text{st.} \quad E(\sigma) = b_V \\ \quad \quad B(\sigma) = b_S \\ \quad \quad F(\sigma) \leq 0 \end{array} \right\} \quad (1)$$

In the equation:

$\sigma$  – Stress field, the independent variable;

$Q(\sigma)$  – Objective function;

$b_V$  – Unit body force;

$E(\sigma) = b_V$ , Equilibrium differential equation;

$B(\sigma) = b_S$ , Stress boundary conditions;

$F(\sigma) \leq 0$ , Yield criterion constraint.

From Equation (1), it can be observed that the lower bound model is an optimization model with both equality and inequality constraints.

### 3 Numerical Solution for the Lower Bound Model

Due to the complexity of practical problems, obtaining an analytical solution for the lower bound model is often challenging. In engineering, numerical methods are commonly employed. Taking the example of a plane strain problem, a mesh is created using quadrilateral elements. The stresses at all nodes are taken as independent variables. The objective function, equilibrium differential equation, stress boundary conditions, and yield criterion constraints from Equation (1) are linearized. This linearization results in a linear programming model. Solving the linear programming model provides the ultimate load for the respective problem. The details are described below.

#### 3.1 Mesh Generation

For the plane strain problem, a mesh is generated using quadrilateral elements. Let there be a total of  $N$  nodes and  $M$  elements in the mesh.

#### 3.2 Independent Variables

The stress components at all nodes are considered as the independent variables and are denoted as  $\sigma_n$ . Since there are  $N$  nodes in the mesh,  $\sigma_n$  is a  $3N$ -dimensional column vector.

#### 3.3 Objective Function

For the linearized objective function, it can be generally represented as:

$$C^T \sigma_n \tag{2}$$

where  $C^T$  is the objective vector.

#### 3.4 Equilibrium Equations

For the element under the action of body forces and surrounding stresses, equilibrium must be maintained in the  $X$  and  $Y$  directions. Assuming the stress distribution on the element's boundaries is linear, the stress distribution in the  $X$  direction on the element's boundary is shown in Figure 1, and the stress distribution in the  $Y$  direction on the element's boundary is shown in Figure 2. The equilibrium equations for the element in the  $X$  and  $Y$  directions can be expressed as follows:

$$[A^e][\sigma^e] = [b^e] \tag{3}$$

In the equation:

$$[A^e] = \begin{bmatrix} \eta_1 & 0 & \zeta_1 & \eta_2 & 0 & \zeta_2 & \eta_3 & 0 & \zeta_3 & \eta_4 & 0 & \zeta_4 \\ 0 & \zeta_1 & \eta_1 & 0 & \zeta_2 & \eta_2 & 0 & \zeta_3 & \eta_3 & 0 & \zeta_4 & \eta_4 \end{bmatrix};$$

$$[\sigma^e] = [\sigma_{x1} \quad \sigma_{y1} \quad \tau_{xy1} \quad \sigma_{x2} \quad \sigma_{y2} \quad \tau_{xy2} \quad \sigma_{x3} \quad \sigma_{y3} \quad \tau_{xy3} \quad \sigma_{x4} \quad \sigma_{y4} \quad \tau_{xy4}];$$

$$\begin{aligned}
 [b^e] &= [Ag_x \quad Ag_y]^T; \\
 \eta_1 &= \frac{1}{2}(y_2 - y_4); \quad \eta_2 = \frac{1}{2}(y_3 - y_1); \\
 \eta_3 &= \frac{1}{2}(y_4 - y_2); \quad \eta_4 = \frac{1}{2}(y_1 - y_3); \\
 \zeta_1 &= \frac{1}{2}(x_4 - x_2); \quad \zeta_2 = \frac{1}{2}(x_1 - x_3); \\
 \zeta_3 &= \frac{1}{2}(x_2 - x_4); \quad \zeta_4 = \frac{1}{2}(x_3 - x_1).
 \end{aligned}$$

where  $A$  is the element area,  $g_x$  and  $g_y$  are the gravitational accelerations in the  $X$  and  $Y$  directions, respectively.

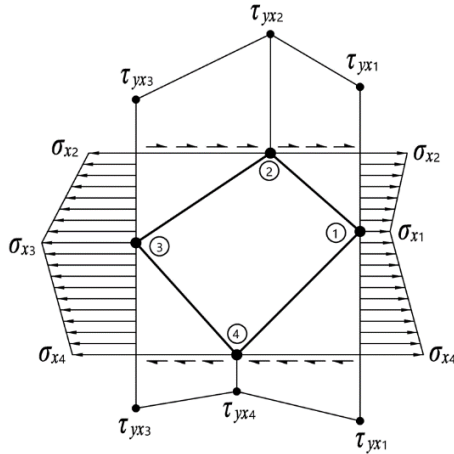


Fig. 1. Stress along the element boundary in X direction.

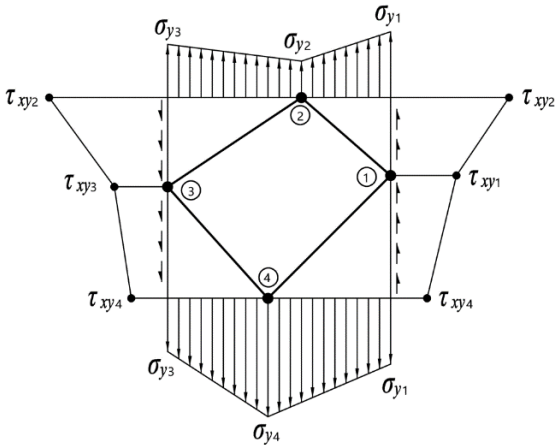


Fig. 2. Stress along the element boundary in the Y direction

Integrating the equilibrium equations for all elements, we can obtain the general form of the overall equilibrium equations as follows:

$$A_1\sigma_n = b_1 \quad (4)$$

### 3.5 Stress Boundary Conditions

Stress boundary conditions essentially represent equality constraints applied to the stresses. Utilizing linearized stress boundary conditions, they can be generally denoted as:

$$A_2\sigma_n = b_2 \quad (5)$$

### 3.6 Yield Criterion

The Mohr-Coulomb yield criterion can be expressed as follows:

$$(\sigma_x - \sigma_y)^2 + (2\tau_{xy})^2 - [2c \cdot \cos\varphi - (\sigma_x + \sigma_y)\sin\varphi]^2 \leq 0 \quad (6)$$

In the coordinate system of  $\sigma_x$ ,  $\sigma_y$ , and  $\tau_{xy}$ , the region represented by Equation (6) is an ellipsoidal cone. Utilizing an inscribed polyhedral cone approximation, Equation (6) can be written as<sup>[11]</sup>:

$$A_k\sigma_x + B_k\sigma_y + C_k\tau_{xy} \leq D \quad (7)$$

In the equation:

$$\begin{aligned} A_k &= \cos(2\pi k/p) + \sin\varphi\cos(\pi/p); \\ B_k &= \sin\varphi\cos(\pi/p) - \cos(2\pi k/p); \\ C_k &= 2\sin(2\pi k/p); \\ D &= 2cc\cos\varphi\cos(\pi/p); \\ k &= 1, 2, \dots, p. \end{aligned}$$

All nodal stresses must satisfy the yield criterion. By integrating all linearized nodal stress yield criterion constraints, the linearized yield criterion constraints can be generally denoted as:

$$A_3\sigma_n \leq b_3 \quad (8)$$

### 3.7 Linearized Model and Solution

Combining the objective function in Equation (2), equilibrium equations in Equation (4), stress boundary conditions in Equation (5), and yield criterion in Equation (8), the linearized model for the lower bound theorem can be generally written as:

$$\left. \begin{array}{l} \max \quad C^T\sigma_n \\ \text{st.} \quad A_1\sigma_n = b_1 \\ \quad \quad A_2\sigma_n = b_2 \\ \quad \quad A_3\sigma_n \leq b_3 \end{array} \right\} \quad (9)$$

In this equation:

$\sigma_n$  – Independent variable, nodal stresses;

$C^T$  – Objective vector;

$A_1\sigma_n = b_1$ – Equilibrium equations;

$A_2\sigma_n = b_2$ – Stress boundary conditions;

$A_3\sigma_n \leq b_3$ – Yield criterion.

Equation (9) represents a linear programming model with both equality and inequality constraints, which can be solved using linear programming software.

### 4 Active Earth Pressure for Cohesionless Soil with Finite Width

The finite width, cohesionless soil discussed in this paper specifically refers to the rectangular area with a height of  $H$  and width  $B$ , as shown in Figure 3. The resultant force of active earth pressure mentioned here specifically refers to the minimum value of the horizontal component of the earth pressure exerted by the soil on the left wall  $L_2$  (positive for compression). The distribution of active earth pressure refers to the corresponding earth pressure distribution acting on the left wall  $L_2$  corresponding to the resultant force of active earth pressure.

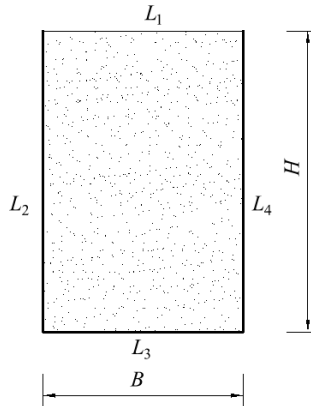


Fig. 3. Cohesionless soil with finite width

The lower bound model described in Section 2 is utilized for this case study. In this example, the given width of the soil ( $B$ ) is 10 m, and the height of the soil ( $H$ ) is taken as 10 m, 20 m, 30 m, 40 m, 50 m, 60 m, 70 m, 80 m, and 90 m. The unit weight of the soil is 18 kN/m<sup>3</sup>, cohesion ( $c$ ) is 0, and the internal friction angle ( $\varphi$ ) is 36°. There is no cohesion and a friction angle of  $\varphi=36^\circ$  between the soil and the walls  $L_2$ ,  $L_3$ , and  $L_4$ . At the upper surface  $L_1$  of the soil, both the vertical normal stress and the horizontal shear stress are zero.

The numerical solution method for the lower bound model described in Section 3 is applied. For this example, the mesh is partitioned as follows: divided into ten

elements in the horizontal direction, with a horizontal width of 1.0m for each element; divided into H elements in the vertical direction, with a vertical height of 1.0m for each element, as shown in Figure 4.

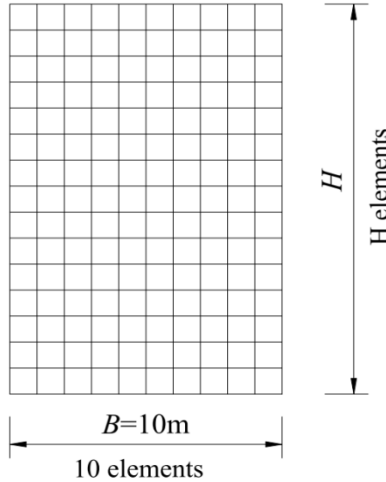


Fig. 4. Mesh of cohesionless soil with finite width

## 5 Calculation Results and Analysis

### 5.1 Total Active Earth Pressure

The total active earth pressure obtained through the lower bound method for different soil heights (H) with a soil width of  $B=10$  m is shown in Table 1. For comparison, the corresponding Coulomb active earth pressure is also provided in Table 1.

From Table 1, it can be observed that the total active earth pressure obtained through the lower bound method increases with the height of the soil, but it is less than the corresponding Coulomb active earth pressure.

The relationship between the total active earth pressure obtained through the lower bound method and the soil height is shown in Figure 5. For comparison, Figure 5 also depicts the relationship between the corresponding Coulomb active earth pressure and the soil height.

From Figure 5, it can be seen that the trend of the total active earth pressure obtained through the lower bound method with respect to soil height is significantly slower compared to the increasing trend of Coulomb active earth pressure with respect to soil height.

**Table 1.** Active pressure in different heights of soil

Soil Height $H$ (m)	Active earth pressure obtained through the lower bound method (MN)	Coulomb active earth pressure (MN)
10	0.18	0.22
20	0.72	0.87
30	1.53	1.95
40	2.49	3.47
50	3.56	5.43
60	4.69	7.82
70	5.86	10.64
80	7.06	13.90
90	8.27	17.59

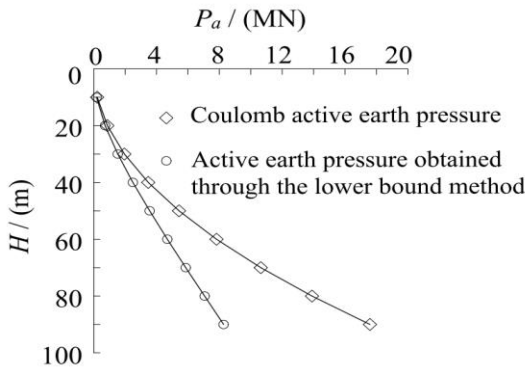


**Fig. 5.** Relationship between active pressure and soil height

**5.2 Distribution of Active Earth Pressure**

The distribution of active earth pressure obtained through the lower bound method for different soil heights ( $H$ ) with a soil width of  $B=10$  m is shown in Figure 6. For comparison, the corresponding distribution of Coulomb active earth pressure is also provided in Figure 6.

The distribution of active earth pressure obtained through the lower bound method for a soil width of  $B=10$  m and a soil height of  $H=90$  m is shown in Figure 7. For comparison, the corresponding distribution of Coulomb active earth pressure is also provided in Figure 7.

From Figure 6 and Figure 7, it can be observed that the active earth pressure obtained through the lower bound method increases with the depth of the soil and tends towards a certain limit value,  $P_{lim}$ . For different soil heights, the soil pressure at the same depth shows consistency. Near the bottom of the soil, within a certain range, there is a slight fluctuation in the earth pressure due to the influence of the computational model and boundaries.

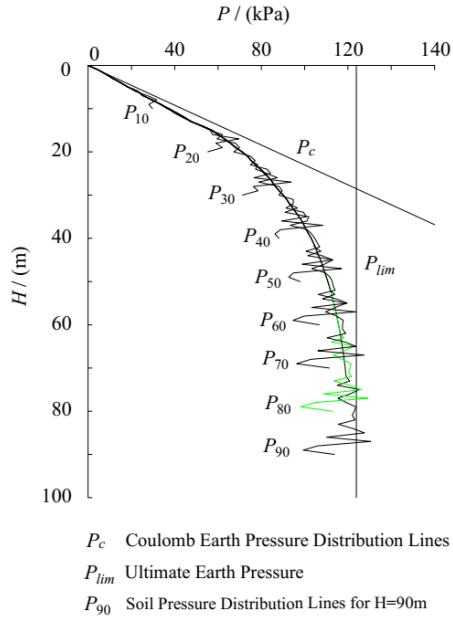


**Fig. 6.** Active press distribution under different soil heights

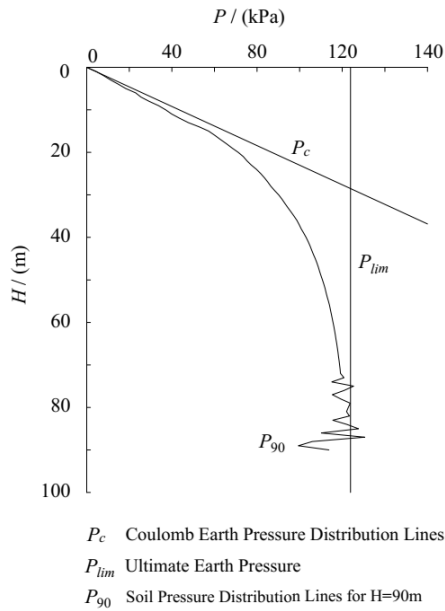


**Fig. 7.** Active press distribution with soil height 90m

The limiting value of earth pressure,  $P_{lim}$ , for a soil with finite width can be understood as follows: as the depth of the soil increases, the lateral pressure exerted by the soil on the retaining wall continuously increases. The vertical frictional force between the soil and the wall also increases accordingly. Ultimately, a balance is reached between the weight of the soil and the vertical frictional force between the soil and the wall, as shown in Figure 8.

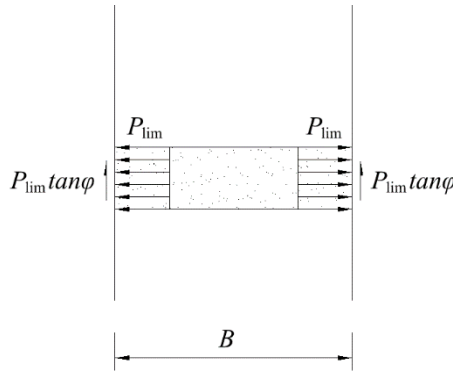


Fig. 8. Active press distribution with soil height 90m

The corresponding limit value of earth pressure associated with this equilibrium state should be:

$$P_{lim} = \frac{\gamma B}{2 \tan \phi} \tag{10}$$

For this example, with  $B=10$  m,  $\gamma=18$  kN/m<sup>3</sup>,  $\phi=36^\circ$ , the calculated  $P_{lim}$  is approximately 123.87 kPa. This limit value is presented in Figure 6 and Figure 7. It can be observed from Figure 6 and Figure 7 that the calculated results using the lower bound method are consistent with the limit value calculated based on Equation (10).

## 6 Conclusion

This article only takes finite width soil pressure as an example, and actually provides a general method to creat serial equilibrium stress field. Based on this method, a general numerical solution for the lower bound theorem is provided. So the lower bound theorem and the corresponding numerical solution method presented in this paper can be applied not only to solve earth pressure problems but also to address issues related to foundation bearing capacity, slope stability, and underground cavity stability.

## References

1. Wang Xiaogang, Lin Xingchao. Limit analysis method for slope stability based on discretization of rigid blocks [J]. Chinese Journal of Geotechnical Engineering, 2022, 44(9): 1587-1597.
2. Lai Fengwen, Liu Songyu, Yang Dayu, Cheng Yuehong, Fan Qinjian. Generalized solution to active earth pressure exerted onto retaining wall with narrow backfills [J]. Chinese Journal of Geotechnical Engineering, 2022, 44(3): 483-491.
3. Chen Qiaofeng, Lei Shengxiang, Zhao Wei, Xiao Qinghua, Li Congming. Study the earth pressure for the limited soil adjacent to underground space in urban based on the asymptotic method [J/OL]. Journal of Railway Science and Engineering.
4. Zhang Zhenbo, Zhou Jiadi, Sun Minglei, Liu Zhichun, Hu Zhinan. Finite soil pressure calculation method of excavation closing to existing underground structure[J/OL]. Journal of Railway Science and Engineering.
5. Xia MingTan. Experimental analysis on mechanical characteristics of narrow backfill behind foundation pit diaphragm wall[J]. Chinese Journal of Underground Space and Engineering, 2022, 18(2): 546-553.
6. Xie Mingxing, Zheng Junjie, Cao Wenzhao, Miao Chenxi. Study of active earth pressure against embankment retaining wall of limited backfill[J]. J. Huazhong Univ. of Sci. & Tech. (Natural Science Edition), 2022, 47(2): 1-6 .
7. Zhang hengzhi, Xu Changjie, He Zhaibing, Huang Zhanjun, He Xiaohui. Study of active earth pressure of finite soils under different retaining wall movement modes based on discrete element method[J]. Rock and Soil Mechanics, 2022, 43(1):257-267.
8. Liu Xinxi, Li Bin, Wang Weiwei, He Cheng, Li Song. Calculation of active earth pressure of finite soil based on layered principal stress trajectory[J]. Rock and Soil Mechanics, 2022, 43(5): 1175-1186.
9. Wang Chongyu, Liu Xiaoping, Cao Zhouhong, Jiang Xu, Zhang Jiaqiang. Experimental study on characteristics of active slip surface of limited width soil behind rigid wall [J]. Rock and Soil Mechanics, 2021, 42(11): 2943-2952.
10. Technical specification of retaining and protecting for building foundation excavation DB11/489-2016[S]. 2016.
11. S W. Sloan. Lower bound limit analysis using finite elements and linear programming [J]. International journal for numerical and analytical methods in geomechanics, 1988, 12(1): 61-77.

**Open Access** This chapter is licensed under the terms of the Creative Commons Attribution-NonCommercial 4.0 International License (<http://creativecommons.org/licenses/by-nc/4.0/>), which permits any noncommercial use, sharing, adaptation, distribution and reproduction in any medium or format, as long as you give appropriate credit to the original author(s) and the source, provide a link to the Creative Commons license and indicate if changes were made.

The images or other third party material in this chapter are included in the chapter's Creative Commons license, unless indicated otherwise in a credit line to the material. If material is not included in the chapter's Creative Commons license and your intended use is not permitted by statutory regulation or exceeds the permitted use, you will need to obtain permission directly from the copyright holder.

